Supplementary Material for

Investigation of Ni-Cu-acid multifunctional synergism in NiCu-phyllosilicate catalysts toward 1,4-butynediol hydrogenation to 1,4-butanediol

Changzhen Wang[*a], Xueqing Hai [a], Jia Li [a], Yupeng Liu [a], Xiaosheng Yu[a], Yongxiang Zhao[*a]

a   Engineering Research Center of Ministry of Education for Fine Chemicals, Shanxi University, Taiyuan, 030006, China

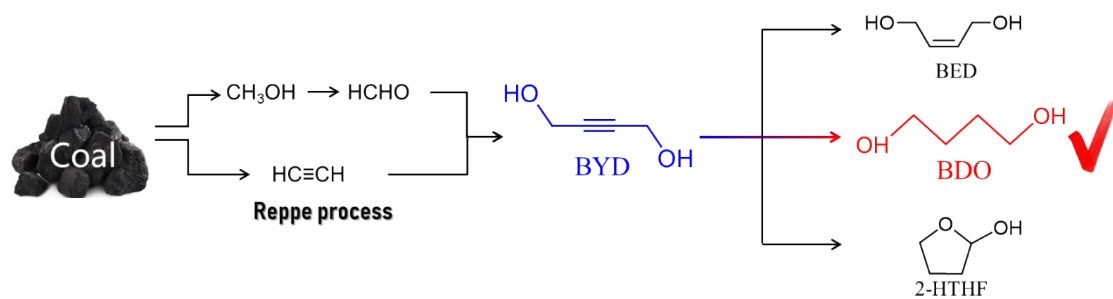*Corresponding authors: czwang@sxu.edu.cn (C. Wang); yxzhao@sxu.edu.cn (Y. Zhao)

Figure S1. Schematic process for the hydrogenation of coal-based 1,4-butynediol and its products network.
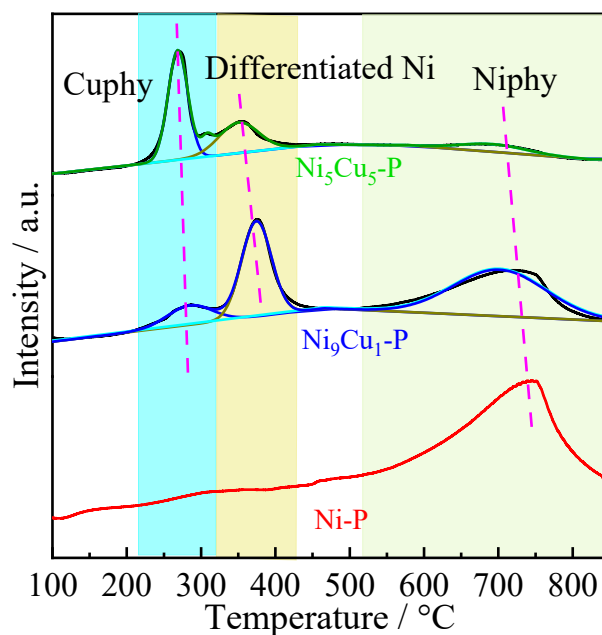
Figure S2. H_2-TPR profiles of Ni-Cu-P catalysts.

Note information: H_2-TPR profiles in Figure S2 provide the information about the Ni-Cu bimetallic synergy as well as the metal support interaction. Due to the distinct phyllosilicate structures of Ni-phyllosilicate (Niphy) and Cu-phyllosilicate (Cuphy), their reduction behaviors are significantly different. According to the former investigations from our and other groups, Cuphy only displayed a sharp peak centered at 290 °C, whereas Niphy displayed a sluggish reduction peak at a rather high and broad reduction temperature range centered at about 720 °C. For the bimetallic Ni_9Cu_1-P catalyst, an obvious three-stage reduction was observed. Notably, the first peak is attributed to the reduction of copper species, and another wide and high temperature reduction stage in the range of 550-800 °C can be designated to Niphy, indicating the stronger metal-support interactions in the phyllosilicate-derived NiCu-P, which can lead to higher metal dispersion and solvothermal-stability of the catalysts[1-2]. Interestingly, there was a new emerged reduction peak at 300-400 °C, which we believe is responsible for the highly active Ni species that differentiated from the Niphy matrix by the induction of promoting Cu species. In general, Cu^{2+} is more easily reducible than Ni^{2+} under similar conditions since it has much lower standard reduction potential[3], and over the Ni-Cu catalyst surface, the presence of Cu species can produce a large

amount of spillover hydrogen which is able to migrate to the adjacent Ni^{2+} sites and consequently accelerates the reduction/nucleation of the nearby Ni site and improves the reducibility of Ni^{2+} species at considerably lower temperatures[4]. As a result, the Ni species bonding to the nearby Cu site has a strong bimetallic synergy effect, and is more reducible at a rather low temperature for NiCu-P. However, as the increase of Cu/Ni ratios will by no means lead to the decline of total active Ni sites number, and Ni_9Cu_1-P showed the largest amount of Cu-induced Ni^0 species differentiated from the Niphy matrix as shown in Figure S2, which may be responsible for its superior hydrogenation activity.
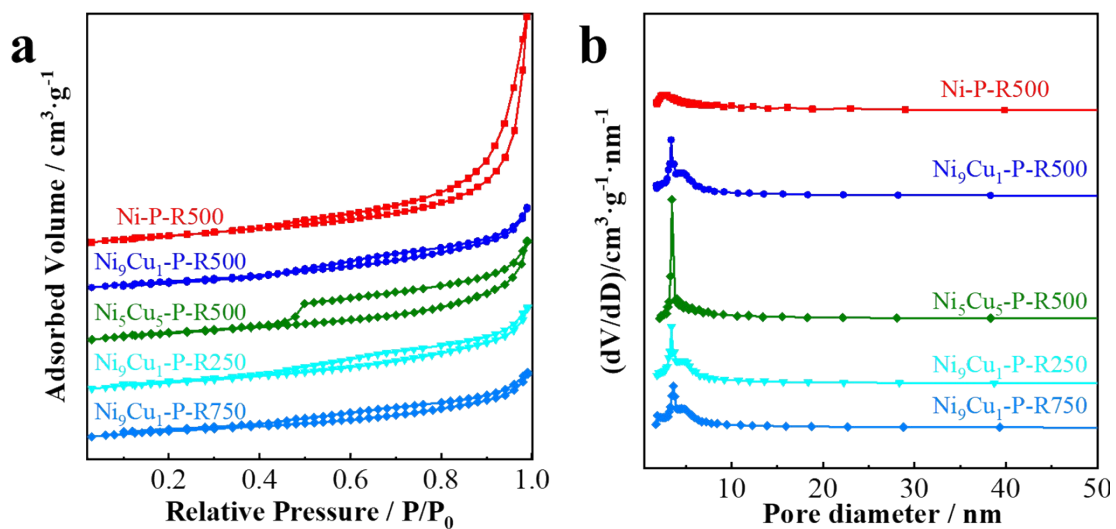
Figure S3. a) N_2 adsorption-desorption isotherms and b) pore size distributions of different reduced catalysts.
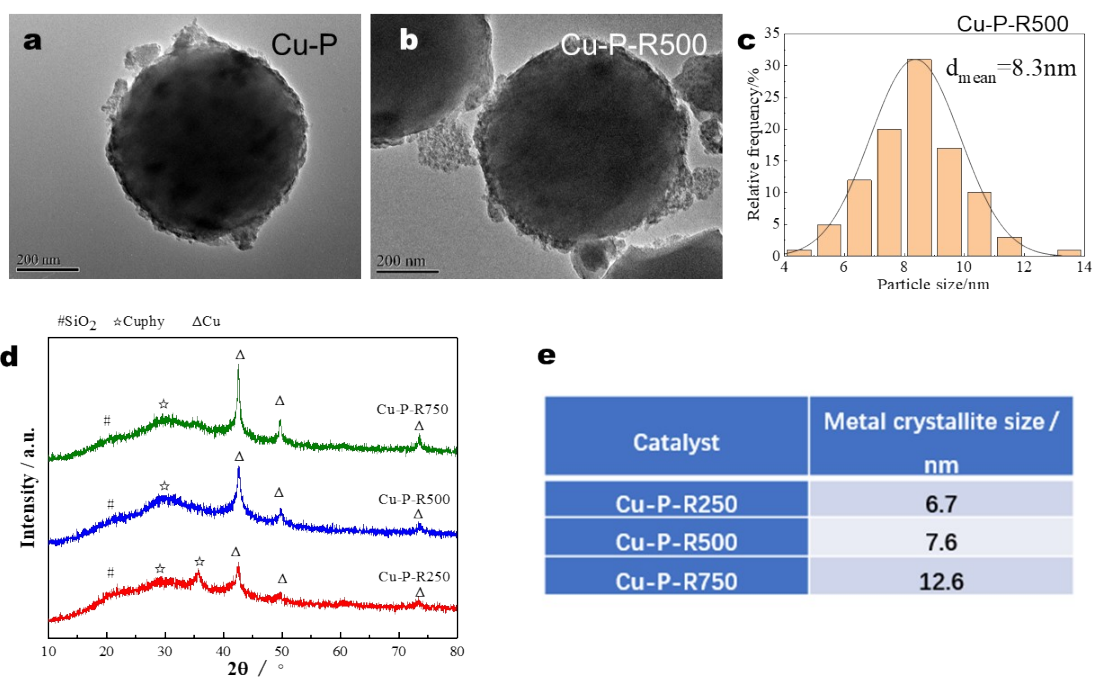
Figure S4. TEM images of a referential Cu-P catalyst a) calcined and b) reduced at 500 °C. c) the mean metal particle size of Cu-P-R500 calculated by counting for more than 100 of the reduced Cu nanoparticles. d) and e) XRD patterns and the corresponding Cu crystalline sizes of the reduced Cu-P catalysts.

Table S1 Metal elemental and species compositions for Ni-Cu-P catalysts.

Catalysts	Metal content [a] / wt%		Metal species composition according to TPR peak fitting [c]/ wt% (%)		
	Cu	Ni	Cu from phy	Diff. Ni	Ni from phy
Ni-P	0	15.9	-	-	15.9(100.0)
Ni_9Cu_1-P	1.6	15.0	1.8(10.7) [b]	5.9(35.5)	8.9(53.8)
Ni_5Cu_5-P	8.5	7.8	9.1(56.0)	5.0(31.2)	2.1(12.8)

a The actual metal content was calculated by XRF.

b The data in parentheses is the metal species percentage integrated from the TPR peak fitting profiles.

c The metal species' composition is quantified according to their TPR percentage in the total metal content.

Table S2. Mean metal particle size at different reduction temperatures.

Catalysts	Mean metal particle size / nm		
	R250	R500	R750
Ni-P	6.3	10.1	12.0
Ni_9Cu_1-P	5.8	8.8	12.3
Ni_5Cu_5-P	3.5	5.6	10.1

Table S3 Textural property of the reduced catalysts.

Catalysts	BET surface area /cm^{2}g^{-1}	Pore volume /cm^{3}g^{-1}	Pore diameter / nm
Ni-P-R500	128.1	0.29	9.2
Ni$_9$Cu$_1$-P- R500	117.1	0.26	8.7
Ni$_5$Cu$_5$-P- R500	129.3	0.31	9.6
Ni$_9$Cu$_1$-P- R250	117.0	0.28	8.7
Ni$_9$Cu$_1$-P- R750	114.4	0.21	7.2

Table S4 Catalyst activity and selectivity tests for BYD hydrogenation over Cu-P-Rx catalysts.

Catalyst	Conversion / %	Product selectivity / %			
		BDO	BED	HTHF	Others
Cu-P-R250	0	-	-	-	-
Cu-P-R500	1.5	0	100	0	0
Cu-P-R750	0	-	-	-	-

Table S5 The peak temperature and desorded H_2 amount for NiCu-P catalysts.

Catalysts	Peak temperature / °C		Amount of desorbed H_2 / mmol g^{-1}
	α-H	β-H	
Ni-P-R250	82	-	0.06
Ni-P-R500	76	-	0.08
Ni-P-R750	74	-	0.10
Ni$_9$Cu$_1$-P-R250	81	122	0.09
Ni$_9$Cu$_1$-P-R500	79	109	0.12
Ni$_9$Cu$_1$-P-R750	76	-	0.05
Ni$_5$Cu$_5$-P-R250	81	124	0.09
Ni$_5$Cu$_5$-P-R500	78	113	0.06
Ni$_5$Cu$_5$-P-R750	75	-	0.05

Table S6 Peak profiles and total acidity for NiCu-P catalysts according to NH_3-TPD results.

Catalysts	Peak temperature / °C		Total acidity / umol g^{-1}
	Weak acid	Medium strong acid	
Ni-P-R250	104	-	1.4
Ni-P-R500	93	265	0.82
Ni-P-R750	92	-	0.39
Ni$_9$Cu$_1$-P-R250	103	-	1.38
Ni$_9$Cu$_1$-P-R500	91	248	0.75
Ni$_9$Cu$_1$-P-R750	94	-	0.43
Ni$_5$Cu$_5$-P-R250	108	-	2.62
Ni$_5$Cu$_5$-P-R500	98	231	0.67
Ni$_5$Cu$_5$-P-R750	102	-	0.46

Table S7 Metal elemental composition of the fresh and spent catalysts after the cycling tests.

Catalysts	Metal content [a]	
	Ni / wt%	Cu / wt%
Ni-P-fresh	15.9	-
Ni-P-1-time-usage	15.8	-
Ni_9Cu_1-P-fresh	15.0	1.6
Ni_9Cu_1-P-3-time-usage	15.2	1.5
Ni_9Cu_1-P-6-time-usage	14.9	1.6
Ni_5Cu_5-fresh	7.8	8.5
Ni_5Cu_5-P-1-time-usage	7.6	8.3

[a] The metal content was detected by XRF results.

References

1.   Kong X; Zhu Y; Zheng H; Li X; Zhu Y; Li Y-W, Ni nanoparticles inlaid nickel phyllosilicate as a metal–acid bifunctional catalyst for low-temperature hydrogenolysis reactions. ACS Catalysis **2015,** *5* (10), 5914-5920.

2.   Sasaki T; Ichikuni N; Hara T; Shimazu S, Study on the promoting effect of nickel silicate for 1-phenylethanol oxidation on supported nio nanocluster catalysts. Catalysis Today **2018,** *307*, 29-34.

3.   Pendem S; Mondal I; Shrotri A; Rao B S; Lingaiah N; Mondal J, Unraveling the structural properties and reactivity trends of cu–ni bimetallic nanoalloy catalysts for biomass-derived levulinic acid hydrogenation. Sustainable Energy & Fuels **2018,** *2* (7), 1516-1529.

4.   Ashok J; Kathiraser Y; Ang M L; Kawi S, Ni and/or ni-cu alloys supported over sio2 catalysts synthesized via phyllosilicate structures for steam reforming of biomass tar reaction. Catalysis Science & Technology **2015,** *5* (9), 4398-4409.